CHAPTER IV
RESULTS AND DISCUSSION

4.1 Bacterial Cellulose

4.1.1 Production of Bacterial Cellulose

Acetobacter xylinum strain TISTR 975 and ATCC 10245, statically inoculated in a suitable culture medium at 30°C, produced bacterial cellulose and formed a thick leather-like white pellicle at the air-liquid interface of the culture medium within 3-7 days as shown in Figure 4.1.

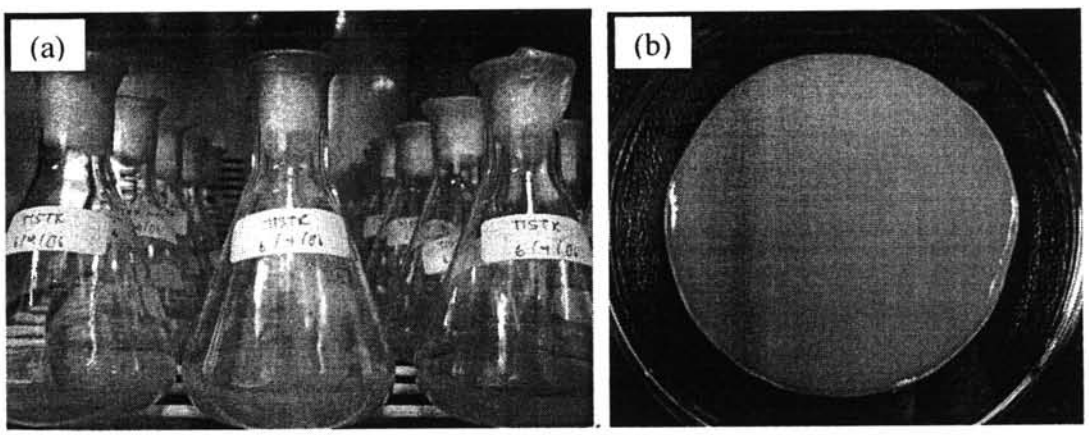

Figure 4.1 Cultivation of *Acetobacter xylinum* strain TISTR 975: (a) under studied conditions and (b) forming of the leather-like white pellicle bacterial cellulose.

During growth and production of bacterial cellulose, the bacterial cells were gradually entrapped in the pellicle. After the initial stage, the formation of the bacterial cellulose took place on the upper site of the cellulose layer. As long as the system was kept unshaken, the disc-shape product was suspended and steadily slide downwards as its thickness was shown in Figure 4.2. After one day of cultivation, the thin gelatinous bacterial cellulose pellicle was formed at the interface of the culture medium. On the third day of cultivation, the bacterial cellulose was already integrated in the gelatinous upper part of the pellicle. And between the fifth

and the seventh day of cultivation the bacterial cellulose were continually covered with a pronounced cellulose layer.

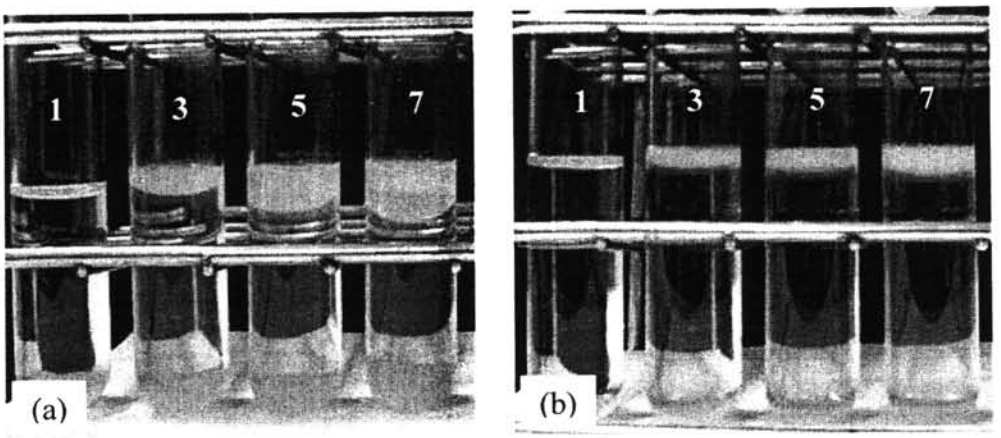

Figure 4.2 Bacterial cellulose pellicles produced under different cultivation time (1, 3, 5, and 7 day) from *Acetobacter xylinum* (a) strain TISTR 975 and (b) strain ATCC 10245.

It is a generally accepted that bacterial cellulose which synthesized and secreted by a highly aerobic *Acetobacter xylinum* can help the bacterial cells to float and reach the oxygen-rich surface (Vandamme *et al.,* 1997). As a result, the bacterial cellulose was formed at the air-liquid interface of culture medium. The mechanism of bacterial cellulose growth is assumed by several scientists. At the initial stage, bacteria increase their population by consumption of oxygen and D-Glucose, initially dissolved in the culture medium, as the carbon source. During this period, bacteria would synthesize a certain amount of bacterial cellulose in liquid phase. However, only bacteria existing in the vicinity of the surface and associate with oxygen can maintain their activity and produce bacterial cellulose. The bacteria below the surface of the pellicle are dormant. They can be reactivated and used as the inoculums for new culture operations (Yoshinaga and Watanabe, 1997; Han and Robyt, 1998). This result was be observed in Figure 4.2 and used to compare as the effectiveness of the bacterial cellulose production.

The effectiveness of the bacterial cellulose production from *Acetobacter xylinum* strain TISTR 975 and strain ATCC 10245 were compared by measurement of the thickness of bacterial cellulose pellicle at a certain time in Figure 4.3. The thickness of bacterial cellulose pellicle produced by *Acetobacter xylinum* strain TISTR 975 significantly increased along with the cultivation time whereas by *Acetobacter xylinum* strain ATCC 10245 slowly produced was observed.

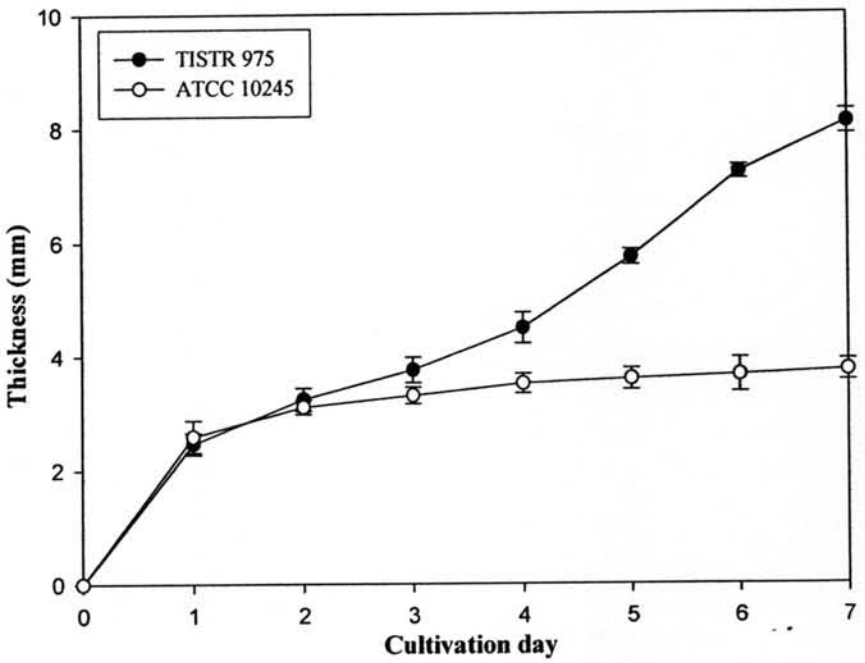

Figure 4.3 Comparison of thickness of bacterial cellulose pellicle produced by -●- *Acetobacter xylinum* strain TISTR 975 and -○- strain ATCC 10245.

At the seventh day of the cultivation, the thickness of bacterial cellulose pellicle, produced by *Acetobacter xylinum* strain TISTR 975 is 8.09 mm where by *Acetobacter xylinum* strain ATCC 10245 is 3.12 mm. Consequently, *Acetobacter xylinum* strain TISTR 975 was used to further studied.

4.1.2 Purification of Bacterial Cellulose

After a certain cultivation time of *Acetobacter xylinum* strain TISTR 975, the leather-like white pellicle of bacterial cellulose at the interface of culture medium was harvested. For purification, the bacterial cellulose pellicle was boiled in a diluted sodium hydroxide (NaOH) to eliminate *Acetobacter xylinum* cells, protein (a by-product during the bacterial metabolism), and the components of the culture medium which entrapped within the bacterial cellulose network (Embuscado, Miller and Marks, 1996). Figure 4.4 shows the yellow-translucent pellicle of untreated-bacterial cellulose became a white-transparent pellicle after purification.

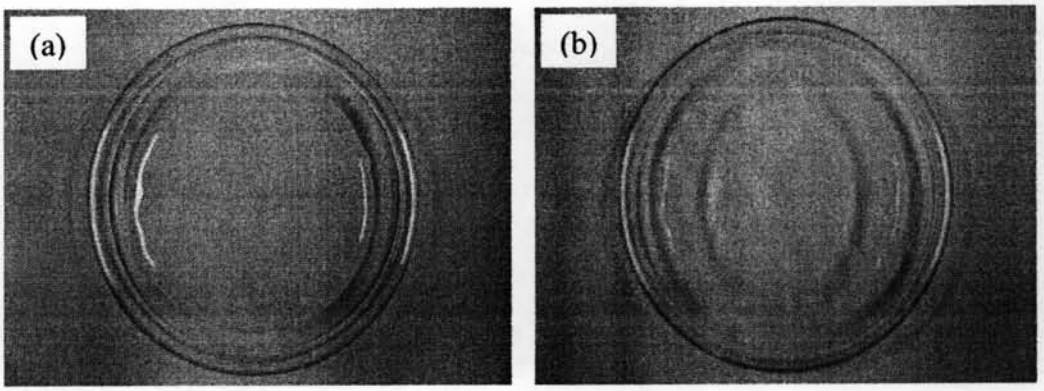

Figure 4.4 Purification of bacteria cellulose: (a) NaOH untreated-bacterial cellulose pellicle (b) NaOH treated-bacterial cellulose pellicle.

In addition, the NaOH treated-bacterial cellulose was investigated by the FT-IR spectra to ensure the purity of bacterial cellulose. Figure 4.5 shows FT-IR spectra of NaOH untreated- and treated-bacterial cellulose pellicle. The FT-IR spectra of the NaOH untreated-bacterial cellulose (Figure 4.5 (a)) show the absorption peak at 1770 cm^{-1}, which performs the strong C=O stretching of the amide I, and at 1634 cm^{-1} which is the weak N-H bending of the amide II. These bonds are the main component of the amino acid, a functional group of protein. This result implies that proteins were entrapped in the bacterial cellulose pellicle. After the bacterial cellulose pellicle was purified by boiling in a diluted-NaOH solution at 90°C for 2 h (2 times), drastic reduction of the amide I and II signal were observed as

shown in Figure 4.5 (b). This result shows that the bacterial cell, protein, and any component of the culture medium were completely eliminated.

The purification result was also confirmed using the SEM images. Figure 4.6 (a) shows the porous structure of NaOH-treated bacterial cellulose compared to the freeze-dried native bacterial cellulose (Figure 4.6 (b)), extensively three dimensional non-woven nanofibrils (Czaja *et al.,* 2004). Additionally, it was observed that NaOH treatment affects the native pellicle by revealing its topological and building a porous structure. Moreover, the intact bacteria and debris were not found in the bacterial cellulose after treatment in contrast with the native bacterial cellulose.

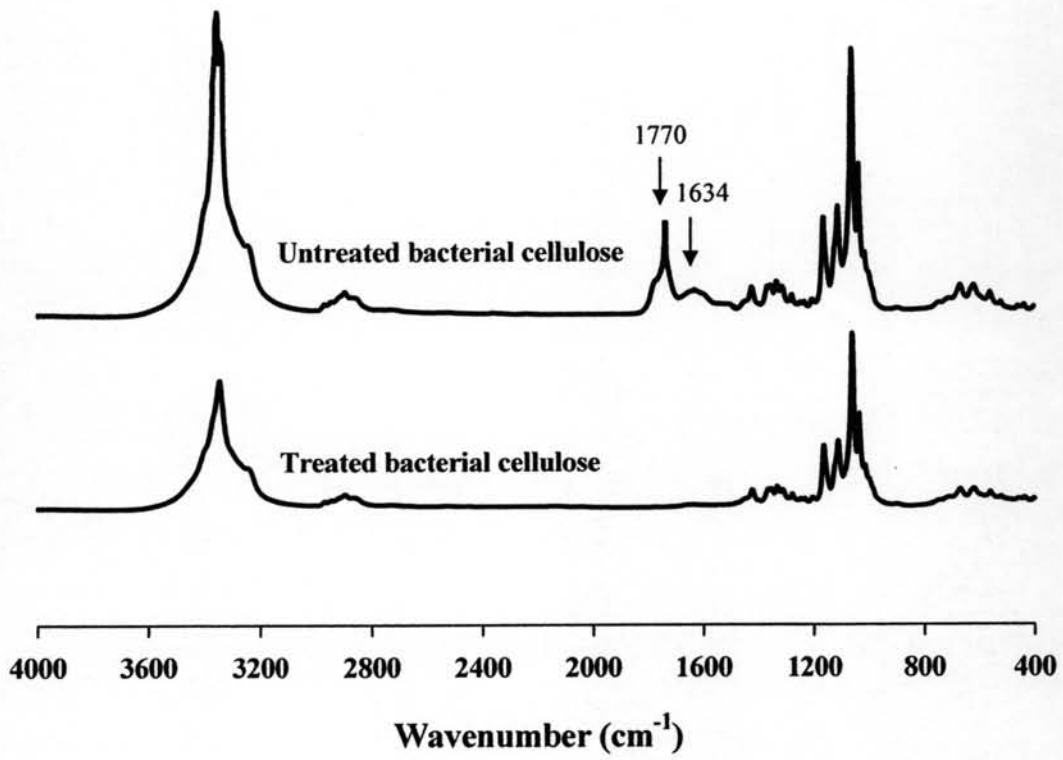

Figure 4.5 FT-IR spectra of (a) NaOH untreated-bacterial cellulose pellicle, (b) NaOH treated-bacterial cellulose pellicle.

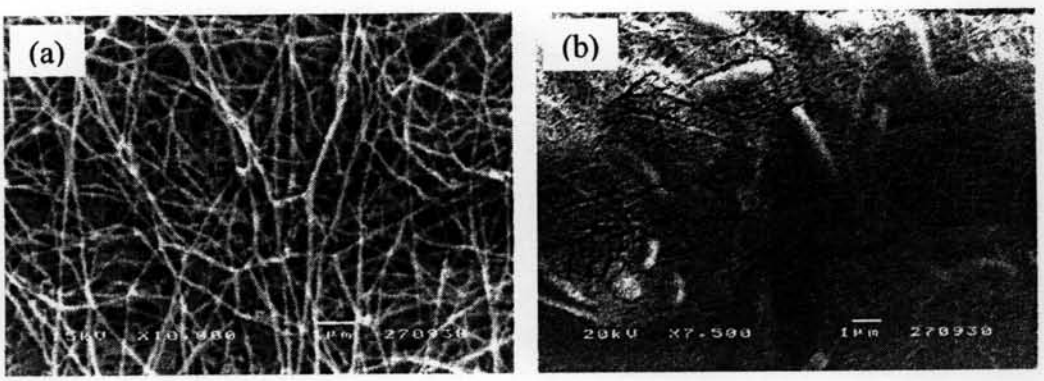

Figure 4.6 SEM image of (a) NaOH-treated bacterial cellulose (x 10000) and (b) NaOH-untreated bacterial cellulose (x 7,500).

4.1.3 Chemical Structure of Bacterial Cellulose

The FT-IR spectra of the plant cellulose and the produced bacterial cellulose were shown in Figure 4.7. The specific wavenumber of FT-IR signals with the possible functional groups are listed in Table 4.1.

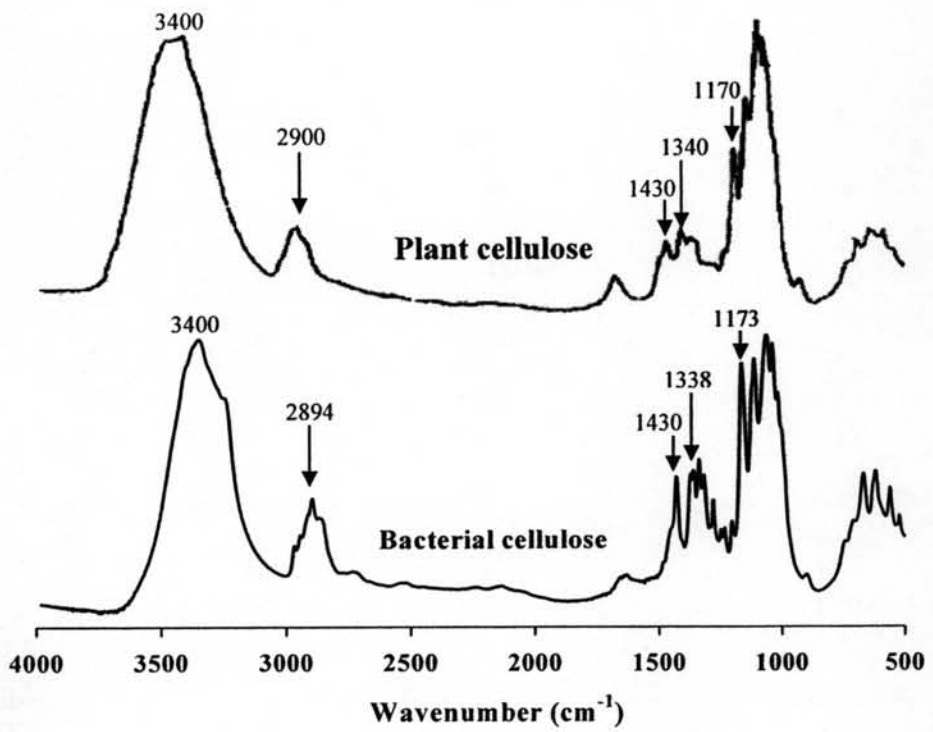

Figure 4.7 FT-IR spectra of the plant cellulose compared to the produced bacterial cellulose.

Table 4.1 Main functional groups of plant and bacterial celluloses

Wavenumber (cm^{-1})	Vibration mode	Functional group
3600-3000	O-H stretching	Hydroxyl (-OH)
2860-2970	C-H stretching	CH_n unit
1430	CH_2 symmetric bending	CH_n unit
1338, 1340	C-H wagging	CH_n unit
1170, 1173	C-O-C stretching	Ether linkage

FTIR spectra of bacterial cellulose show the absorption peak at the same position as a plant cellulose, thus both plant and bacterial celluloses are consisted of the same functional groups and linkage, e.g. the -CH_2, -CH, hydroxyl group (-OH) and ether linkage (C-O-C).

This result shows that the produced bacterial cellulose has the same chemical structure as the plant cellulose, β -1, 4-glucan chain, as shown in Figure 4.8.

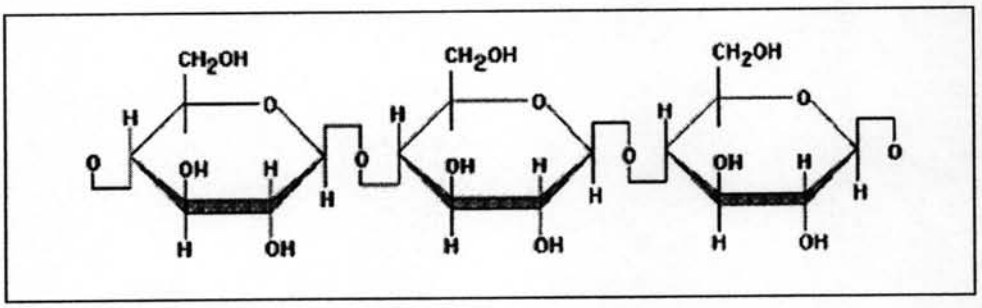

Figure 4.8 Chemical structure of bacterial cellulose.

4.1.4 Morphology of Bacterial Cellulose

SEM images for the surface and cross-section morphology of the bacterial cellulose is shown in Figure 4.9. The three dimensional non-woven structure with many void spaces among nanofibrils network in the surface of bacterial cellulose membrane, is illustrated. The direct measurement indicated that the pore size was in between 0.1 and 5.0 μm with the nanofibrils size of 50 to 150 nm (Figure 4.9 (a)). The multilayer of bacterial cellulose membranes linked together with the nanofibrils is observed in the cross-section morphology of bacterial cellulose as shown in Figure 4.9 (b). This result confirms the mechanism of formation of the bacterial cellulose pellicle; only bacteria exist in the vicinity of the surface and associate with oxygen can produce bacterial cellulose (Wojciech *et al.*, 2004).

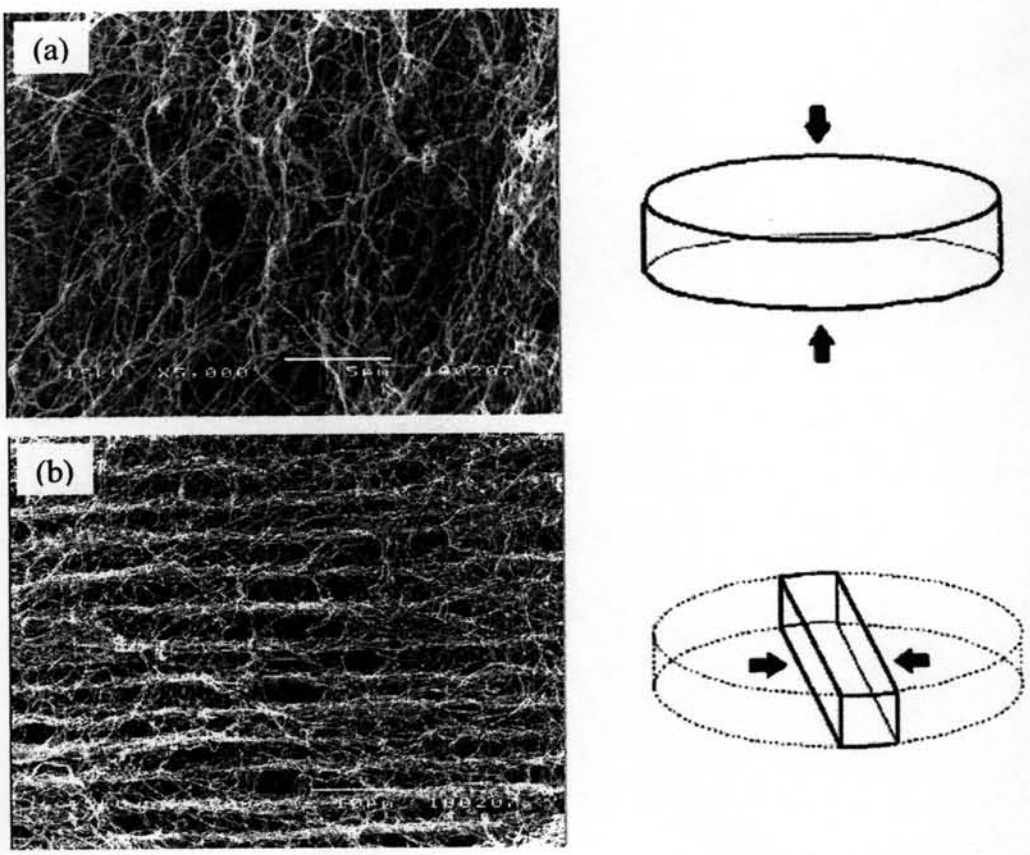

Figure 4.9 SEM images for (a) the surface (X5000) and (b) the cross-section morphology (X2000) of bacterial cellulose.

Bacterial cellulose has the same chemical structure as cellulose that is produced by plant but its structure is completely different. Figure 4.10 show that the produced bacterial cellulose is much smaller than that of the cellulose produced from plant.

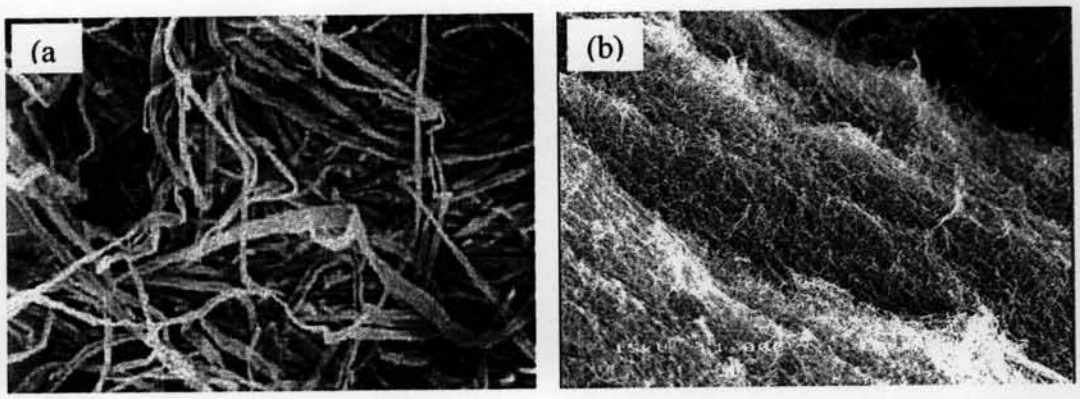

Figure 4.10 Comparison of SEM image (a) of plant cellulose (x200) and (b) of produced bacterial cellulose (x1000).

4.2 Impregnation of Silver Nanoparticles into Bacterial Cellulose

Structure of bacterial cellulose is three-dimensional non-woven networks of nanofibrils with diameter of 50-150 nm and consists of large amount of pores. As bacterial cellulose was immersed in the aqueous solution of $AgNO_3$, the silver ions were readily penetrated into bacterial cellulose though their pores. The incorporation of silver ions (Ag^+) bound to the surface of bacterial cellulose nanofibrils are probably via the electrostatic interactions (He *et al.*, 2003). Since the electron-rich oxygen atoms of polar hydroxyl and ether groups of bacterial cellulose are expected to interact with electropositive transition metal cations. Hence, rinsing with ethanol is an effectively way to remove the excess amount of silver ions. After reduction in the aqueous $NaBH_4$, the absorbed Ag^+ ions were reduced to form the silver nanoparticles on the surface of bacterial cellulose nanofibrils as shown in Figure 4.11. The original colorless bacterial cellulose was turned to yellow. Finally, the silver nanoparticle-impregnated bacterial cellulose was dried by the freeze-drying method to maintain the original structure of bacterial cellulose (Dieter *et al.*, 2001) and to lock up the silver nanoparticles content until the dressing was re-hydrated by moisture or wound exudates.

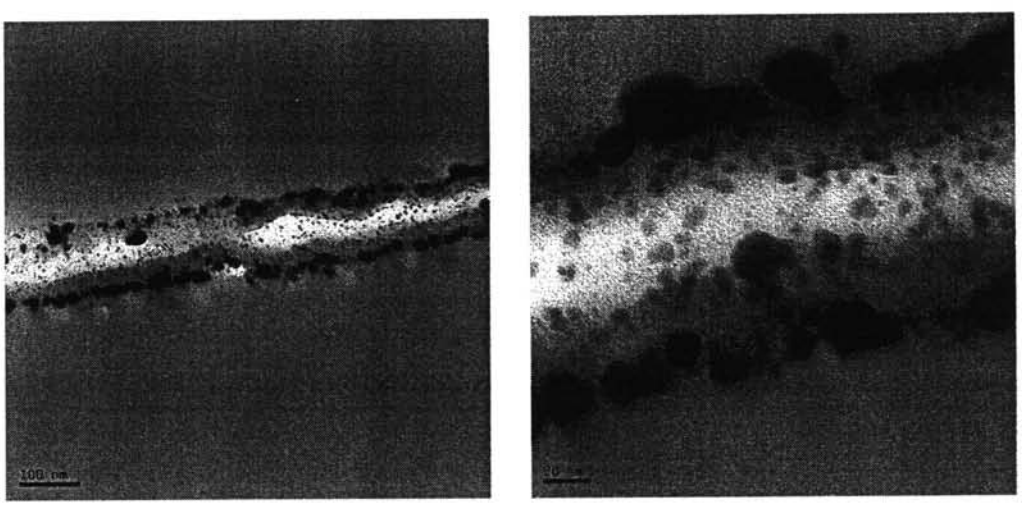

Figure 4.11 TEM image of the single silver nanoparticle-impregnated bacterial cellulose nanofibrils.

The X-ray diffraction (XRD) was used to examine the crystal structure of metal nanoparticles confirming the formation of silver nanoparticles. A typical XRD pattern of silver nanoparticle-impregnated bacterial cellulose was shown in Figure 4.12. It shows four main peaks at 2θ values of 38.1°, 44.3°, 64.4°, and 78.0° corresponding to (111), (200), (220) and (311) planes. This indicates that the high crystallinity and the face centered cubic (fcc) structure of silver nanoparticles (Zhang *et al.*, 2006; Guo-Hua Jiang *et al.*, 2005).

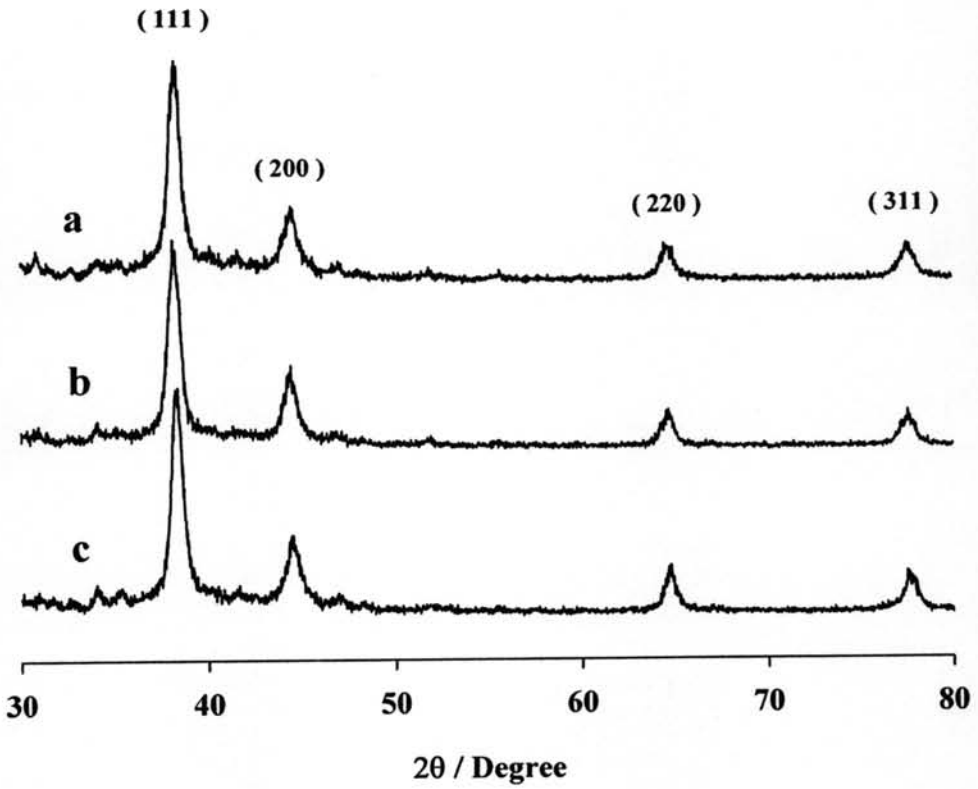

Figure 4.12 The XRD pattern of silver nanoparticle-impregnated bacterial cellulose prepared from the $NaBH_4$: $AgNO_3$ molar ratio of (a) 100 : 1, (b) 10 : 1, and (c) 1 : 1.

Figure 4.13 shows the UV-visible spectra of the silver nanoparticle-impregnated bacterial celluloses. At the $NaBH_4$:$AgNO_3$ molar ratio of 100:1, a narrow symmetrical absorption band is located at 420 nm, the typical absorption of metallic silver nanoparticles due to the surface plasmon resonance (SPR) (HwanKim *et al.*, 2004). No any absorption was observed at wavelengths longer than 500 nm.

This implies that the small silver nanoparticles with the narrow size distribution were formed. The absorption band underwent a red-shift to 428 nm and was slightly broadened at the $NaBH_4$:$AgNO_3$ molar ratio of 10:1. The absorption band underwent a red-shift to 442 nm and became much broadened at the $NaBH_4$:$AgNO_3$ molar ratio of 1:1. The red-shift and broadening of absorption band is possible to show an increase in the particle size and size distribution (Kreibig and Vollmer, 1995; Sconichsen *et al.,* 2002). This suggests that the larger silver nanoparticles with the wider size distribution were probably formed when the $NaBH_4$:$AgNO_3$ molar ratio was decreased, which resulted from the silver ions aggregated together.

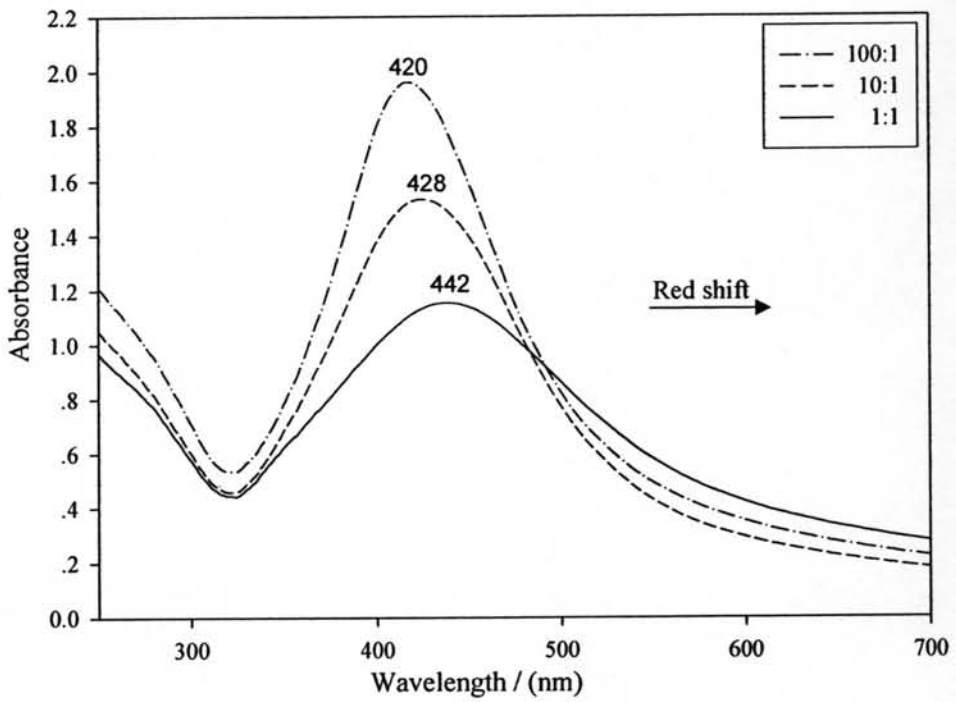

Figure 4.13 Absorption spectra of silver nanoparticle-impregnated bacterial cellulose was prepared from the $NaBH_4$: $AgNO_3$ molar ratio of 1: 1, 10: 1, and 100: 1.

These results are confirmed by the TEM observation. As shown in Figure 4.14 (a) and (b), irregular shapes of silver nanoparticles with the large and wide size distribution were obtained at the $NaBH_4$:$AgNO_3$ molar ratio of 1:1. Their mean diameter (*d*) and standard deviation (σ) were estimated at 11.34 nm and 6.31 nm, respectively. When the $NaBH_4$:$AgNO_3$ molar ratio was increased to 10:1, the particle

size decreased (d = 6.48 nm) and the size distribution became small (σ = 2.68 nm) as shown in Figure 4.14 (c) and (d). The well dispersed and regular spherical silver nanoparticles were obtained at the $NaBH_4$:$AgNO_3$ molar ratio of 100:1. The particle size was much smaller (d = 5.47 nm) and the size distribution became rather narrow (σ = 2.20 nm) as shown in Figure 4.14 (e) and (f). Therefore, the particle size and size distribution of silver nanoparticles are controlled by adjusting the molar ratio of $NaBH_4$ to $AgNO_3$.

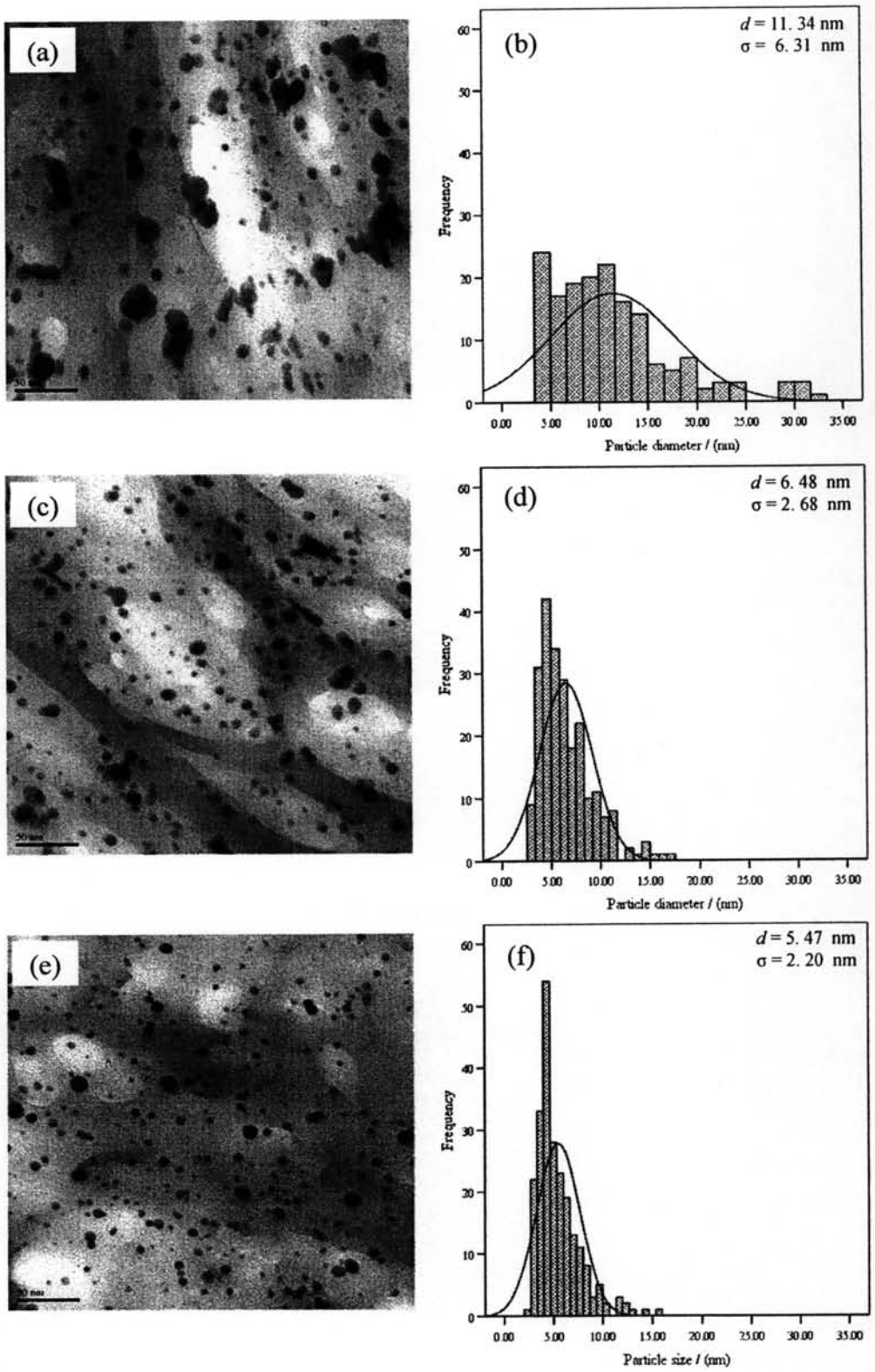

Figure 4.14 TEM images and histograms of silver nanoparticle-impregnated bacterial cellulose was prepared from the $NaBH_4$:$AgNO_3$ molar ratio of 1:1 ((a) and (b)), 10:1 ((c) and (d)), and 100:1 ((e) and, (f)).

Moreover, the $NaBH_4$:$AgNO_3$ molar ratio influenced the depth of silver nanoparticles inside of bacterial cellulose which resulted from the cation concentration gradient between the absorbed Ag^+ inside of bacterial cellulose and the Na^+ of the aqueous $NaBH_4$ outside of bacterial cellulose during the chemical reduction of silver nanoparticles.

At the $NaBH_4$:$AgNO_3$ molar ratio of 1:1, the concentration of absorbed Ag^+ ions inside the bacterial cellulose was equal to that of the Na^+ ions outside the bacterial cellulose. When the Ag^+ ions at the surface of bacterial cellulose were reduced to form the silver nanoparticles, the cat-ion concentration gradient was occurred and the some deeper Ag^+ ions penetrated to the surface and formed nanoparticles. Thus, the silver nanoparticles were formed only at the surface of bacterial cellulose and there are some absorbed Ag^+ inside of bacterial cellulose pellicle.

At the higher $NaBH_4$:$AgNO_3$ molar ratios of 1:1 (10:1 and 100:1) the silver nanoparticles formed inside of bacterial cellulose were deeper, respectively, as shown in Figure 4.15 (b) and (c). Because of the concentration of absorbed Ag^+ ions inside of bacterial cellulose is much lower than concentration of Na^+ ions of the aqueous $NaBH_4$ outside of bacterial cellulose that mean the cat-ion concentration gradient occurred, thus Na^+ ions in the aqueous $NaBH_4$ penetrate into bacterial cellulose pellicles, not Ag^+ ions penetrate out, and then Ag^+ ions were reduced and formed nanoparticles.

On the contrary, at lower $NaBH_4$:$AgNO_3$ molar ratio of 1:1 (1:100), the concentration of absorbed Ag^+ ions in bacterial cellulose pellicle is much more than concentration of Na^+ ions in the aqueous $NaBH_4$ that mean the cat-ion concentration gradient occurred, thus absorbed Ag^+ ions in bacterial cellulose pellicle penetrate out and form nanoparticles in solution, not bacterial cellulose pellicle, that can be observed by the color change of clear solution of aqueous $NaBH_4$ to yellow solution (Figure 4.15 (d)).

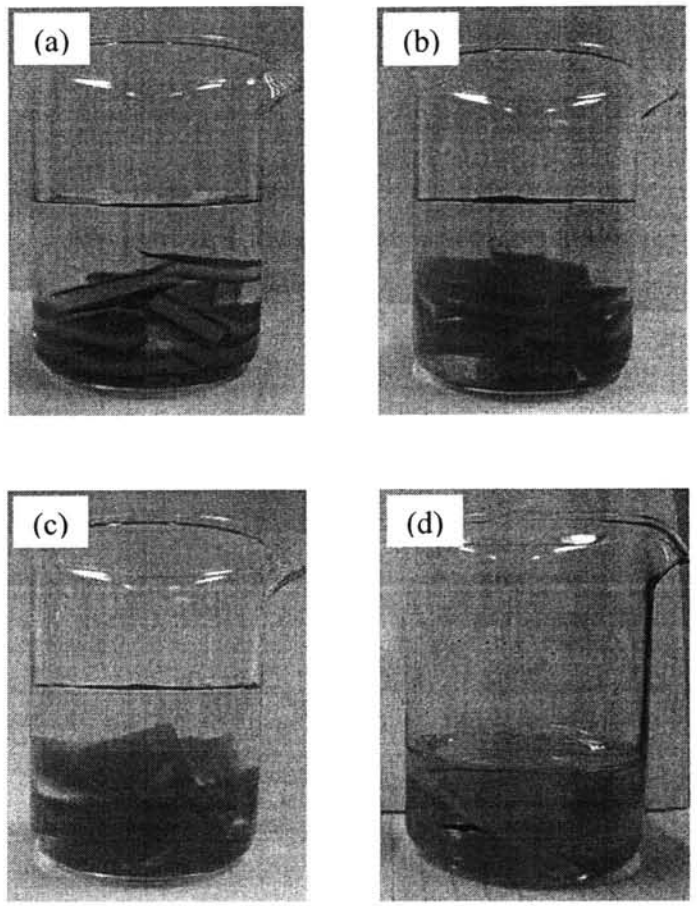

Figure 4.15 The layer of silver nanoparticles impregnated into bacterial cellulose prepared from the $NaBH_4$:$AgNO_3$ molar ratio of (a) 1:1, (b) 10:1, (c) 100:1, and (d) 1:100.

These conclusions were confirmed by Energy Dispersive X-ray (EDX) analysis that used to identify the elemental composition in the sample. As shown in Figure 4.16, the amount of sodium (Na) in the silver nanoparticle-impregnated bacterial cellulose was increased when the $NaBH_4$: $AgNO_3$ molar ratio was increased from 1: 1 to 10: 1 and 100: 1, respectively. The composition of Na and other elements in the silver nanoparticle-impregnated bacterial cellulose prepared from each of the $NaBH_4$:$AgNO_3$ molar ratio were concluded in Table 4.2.

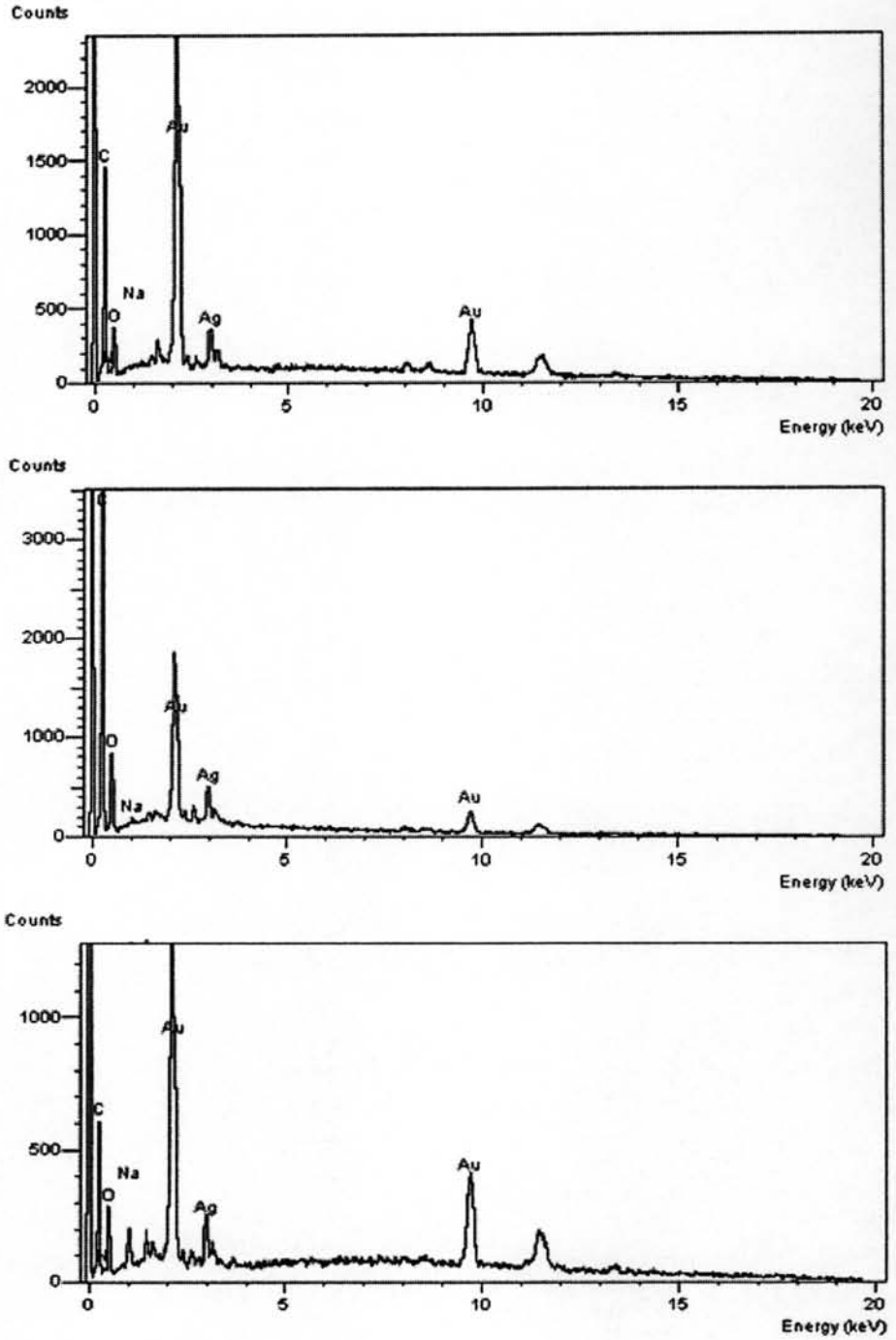

Figure 4.16 EDX spectrum of silver nanoparticles impregnated into bacterial cellulose, prepared from the $NaBH_4$:$AgNO_3$ molar ratio of (a) 1:1, (b) 10:1, (c) 100:1, and (d) 1:100.

Table 4.2 The composition of element in the silver nanoparticles impregnated into bacterial cellulose

$NaBH_4$:$AgNO_3$ Molar ratio	% Element						
	C	O	Na	B	Ag	Au	Total
1: 1	51.18	25.50	0.02	0.00	2.91	20.39	100.00
10: 1	51.85	26.13	0.29	0.00	2.94	18.78	100.00
100:1	43.52	30.38	2.51	0.00	3.35	20.24	100.00

The composition of sodium (Na) in the samples was increased by increasing of the $NaBH_4$: $AgNO_3$ molar ratio that resulted from the cat-ion concentration gradient between sodium ions (Na^+) in the aqueous $NaBH_4$ and absorbed silver ions (Ag^+) in bacterial cellulose pellicle during the chemical reduction of silver nanoparticles whereas boron (B), which is also the main component in the aqueous $NaBH_4$ and can cause the human tissue damage, was not found in these samples. These results implied that after the chemical reduction of silver ions in $NaBH_4$ and washing with large amount of pure water for 10 min, there is only sodium (Na) that was trapped inside of bacterial cellulose.

4.3 Color Change and Distribution of Silver Nanoparticles

After reduction of the absorbed Ag^+ ions, silver nanoparticles were formed inside of bacterial cellulose pellicle. The original colorless of bacterial cellulose was turned to yellow color which is resulted from silver nanoparticles exhibit the characteristic absorption band around 400-500 nm due to the surface plasmon resonance of the free electron on the surface of silver nanoparticles (HwanKim *et al.*, 2004). The absorption band occurred in the range of 400-500 nm or in the blue range of the visible light spectrum, thus silver nanoparticle-impregnated bacterial cellulose show yellow color (Temgire and Joshi, 2004; Zhu *et al.*, 2006).

As shown in Figure 4.17, the color of silver nanoparticle-impregnated bacterial cellulose gradually changed from brown yellow to bright yellow with increasing molar ratio of $NaBH_4$ to $AgNO_3$ from 1:1 to 10:1 to 100:1 that are resulted from the difference of size and size distribution of silver nanoparticles inside of bacterial cellulose.

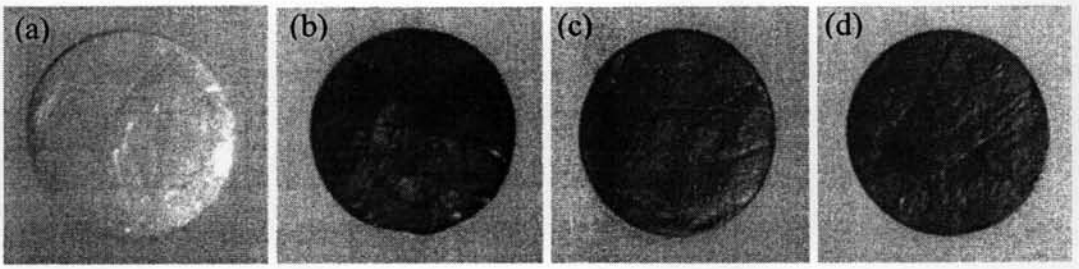

Figure 4.17 The original colorless of pure bacterial cellulose (a) and the yellow color of silver nanoparticle-impregnated bacterial cellulose prepared from the $NaBH_4$: $AgNO_3$ molar ratio of (b) 1: 1, (c) 10: 1, and (d) 100: 1.

Since yellow color of silver nanoparticle-impregnated bacterial cellulose was occurred from the surface plasmon resonance of silver nanoparticles, thus the uniform yellow color of silver nanoparticle-impregnated bacterial cellulose that are shown in Figure 4.17 (b), (c), and (d) can imply that silver nanoparticles were well dispersed throughout bacterial cellulose fiber.

4.4 Silver Content and Releasing Behavior

Silver content of sample those were prepared from the $NaBH_4$: $AgNO_3$ molar ratio of 1:1, 10:1 and 100:1 were measured to be 5.08, 5.20 and 5.22 ppm (mg/L) respectively. Silver content of sample influence the antimicrobial activity and toxicity on the normal human cells. Minimum inhibitory concentrations (MICs) of silver to bacteria range from 0.5-10 ppm whereas minimum bactericidal concentrations (MBCs) range from 2-20 ppm. An additional consideration reports that silver ion concentrations higher than 10 ppm may be toxic to normal human cells (Schierholz *et al.*, 1998). These result implied that these samples can exhibit antimicrobial activity and may not be toxic to the normal human cells.

Figure 4.18 clearly shows that the depth of silver nanoparticles inside the bacterial cellulose affected the silver ions releasing behavior. The silver ions were rapidly released and decreased from the silver nanoparticle-impregnated bacterial cellulose, especially, the nanoparticles prepared from the $NaBH_4$: $AgNO_3$ molar ratio of 1:1. This was due to the silver nanoparticle was impregnated only on the surface of bacterial cellulose. When the $NaBH_4$: $AgNO_3$ molar ratios were increased from 1:1 to 10:1 and 100:1, the impregnated silver nanoparticles were deeper, thus the silver ions were released and decreased slower.

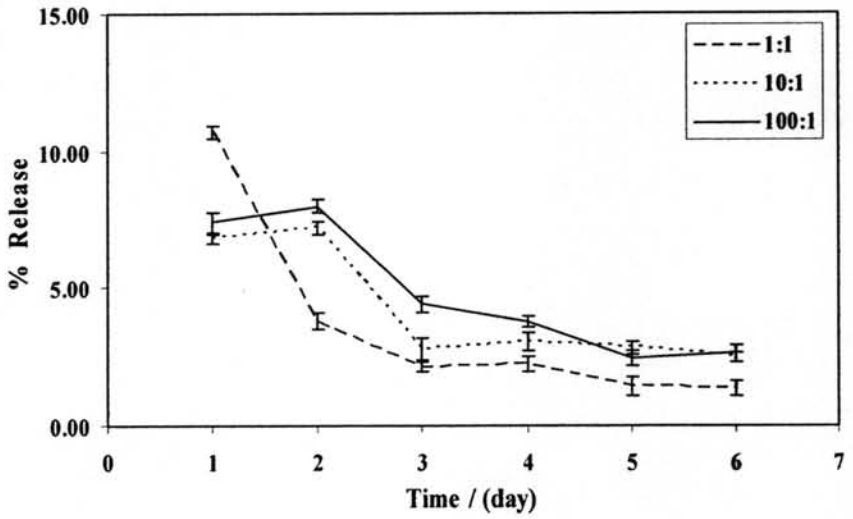

Figure 4.18 Releasing behaviors of silver ions from the silver nanoparticle-impregnated bacterial cellulose.

4.5 Swelling

Figure 4.19 show high swelling ability of silver nanoparticle-impregnated freeze-dried bacterial cellulose, 62.25 of swelling ratio after immersing in the deionized water for 4h that is due to both chemical and physical structure; for chemical structure, bacterial cellulose is hydrophilic material that is expected to absorb molecule of water (Klemm *et al.*, 2001); for physical structure, bacterial cellulose is three dimensional non-woven network with large amount of pores which was maintained by freeze drying method and this physical structure is expected to generate the capillary force within network of bacterial cellulose and suck the molecules of water (Yamanaka *et al.*, 2000). High swelling ability of silver nanoparticle-impregnated bacterial cellulose is important property for wound dressing that used to control wound exudates and keep moist environment on the wound.

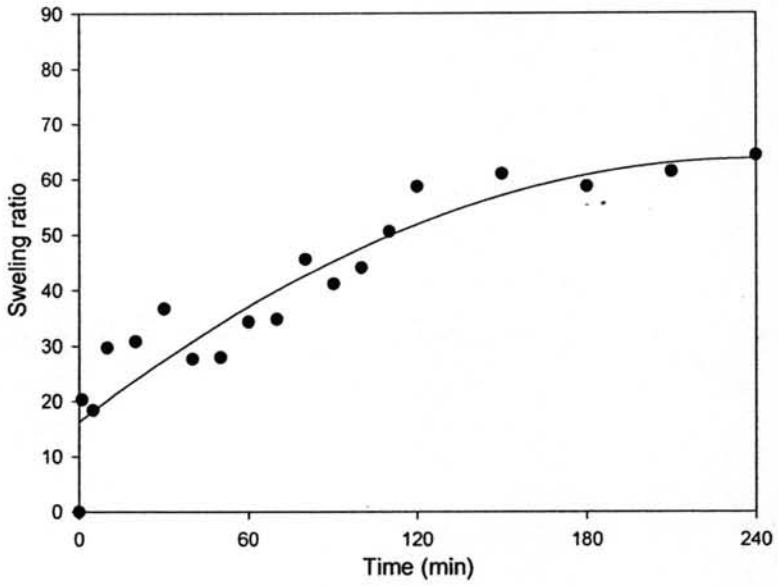

Figure 4.19 Swelling ratio of silver nanoparticle-impregnated bacterial cellulose.

4.6 Mechanical Properties

Figure 4.20 shows a stress-strain response of the silver nanoparticle-impregnated bacterial cellulose in the dry state. Linear elastic behavior is showed between 2.5 and 6.0 % elongations. After this extension the sample is immediately broken. No nanofibrils rearrangement in the direction of force is visualized at deformation as shown in Figure 4.22 (a). Due to the high density of inter- and intra-fibrilar hydrogen bonding of bacterial cellulose nanofibrils that inhibited the motion of nanofibrils. Moreover, a high density of the hydrogen bonding was the source of the strength and also affected the % elongation at break of sample that is only 6 % elongation. This results shows that samples in dried state has high tensile strength but low elasticity. In the hydrate state, the tensile strength and Young's modulus were insignificantly decreased while the percentage of elongation at break point was much increased (Figure 4.21 (a) and (b)) when compared to the sample in the dry state. Because of the density of hydrogen bonding between nanofibrils was lowered that resulted from the penetration of the molecule of water into the network of nanofibrils, thus the nanofibrils mobility was increased resulting in the higher % elongation at break. The rearrangement of nanofibrils in the direction of force is observed in the range of 16 to 30 % elongation. After this rearrangement the sample is gradually broken. Figure 4.22 (b) shows the rearrangement of nanofibrils in the direction of force after the break point.

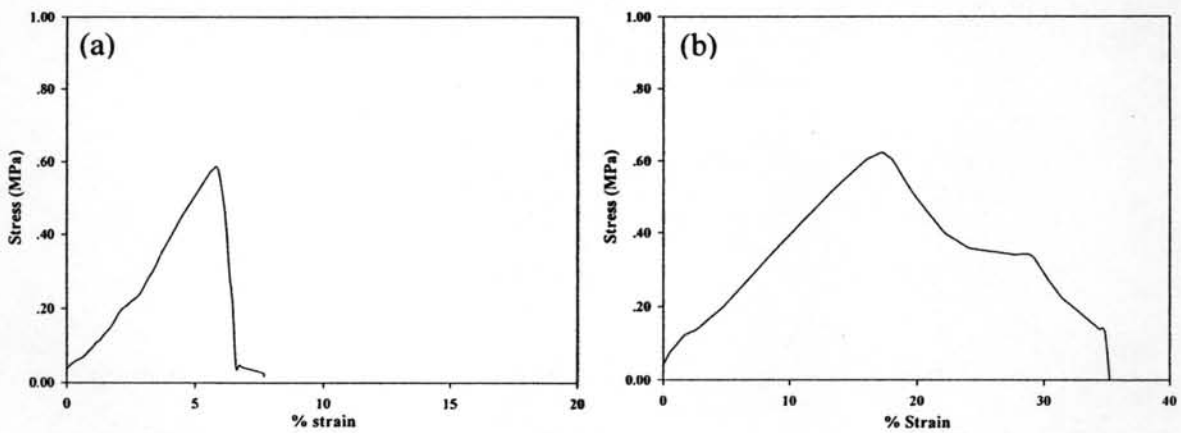

Figure 4.20 Stress/strain diagrams of the silver nanoparticle-impregnated bacterial cellulose in (a) the dry state and (b) the hydrate state.

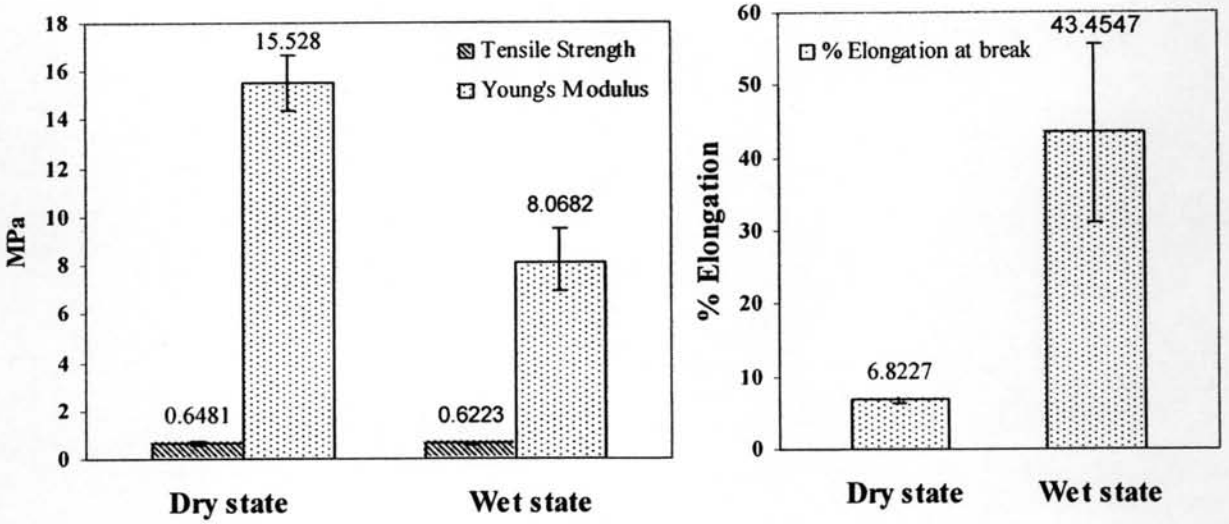

Figure 4.21 shows the values of (a) the tensile strength and Young's modulus, (b) the percentage of elongation at break of the silver nanoparticle-impregnated bacterial cellulose in dry state and wet state.

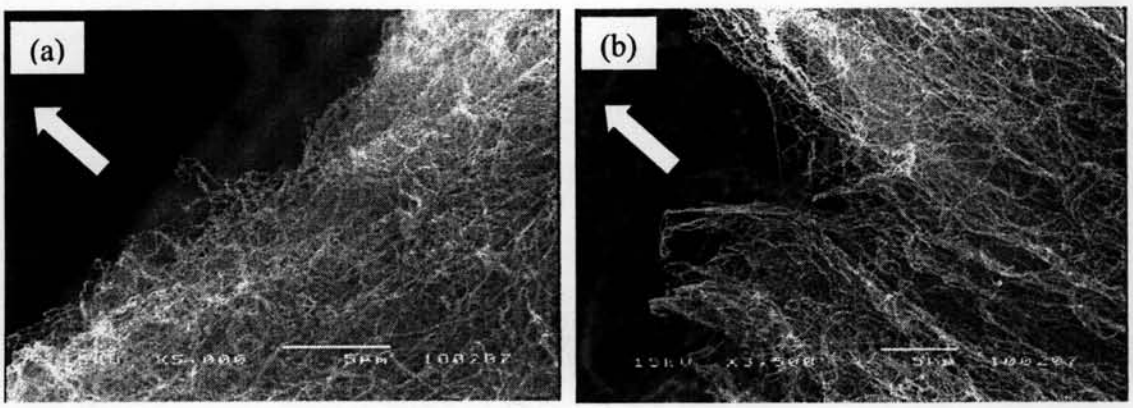

Figure 4.22 SEM image of the bacterial cellulose nanofibrils network closed to fracture: (a) of silver nanoparticle-impregnated bacterial cellulose in the dry state (X5000) and (b) in the hydrate state (X2000) (White-arrows represented the direction of force).

These high tensile strength and high elongation in the hydrated state is useful for this sample because it have to be used in the hydrated state, to activate silver nanoparticles inside of bacterial cellulose.

4.7 Antimicrobial Activity Testing

4.7.1 The Disk Diffusion Method

The antibacterial activity of silver nanoparticle-impregnated bacterial cellulose for *Escherichia coli* and *Staphylococcus aureus* was measured by the disk diffusion method. It was found that the silver nanoparticle-impregnated bacterial cellulose exhibited an inhibition zone. The growth inhibition ring of *Escherichia coli* and *Staphylococcus aureus* was 2 and 3.5mm, respectively. No inhibition zone was observed with the pure bacterial cellulose as control (Figure 4.23). According to the EDX analysis, the silver nanoparticle-impregnated bacterial cellulose only consists of silver nanoparticles and sodium that was trapped inside of bacterial cellulose during chemical reduction in the aqueous $NaBH_4$, but sodium has no antimicrobial activity. This clearly demonstrates that the antimicrobial activity is only due to the silver nanoparticles impregnated in the bacterial cellulose, not due to individual bacterial cellulose and sodium.

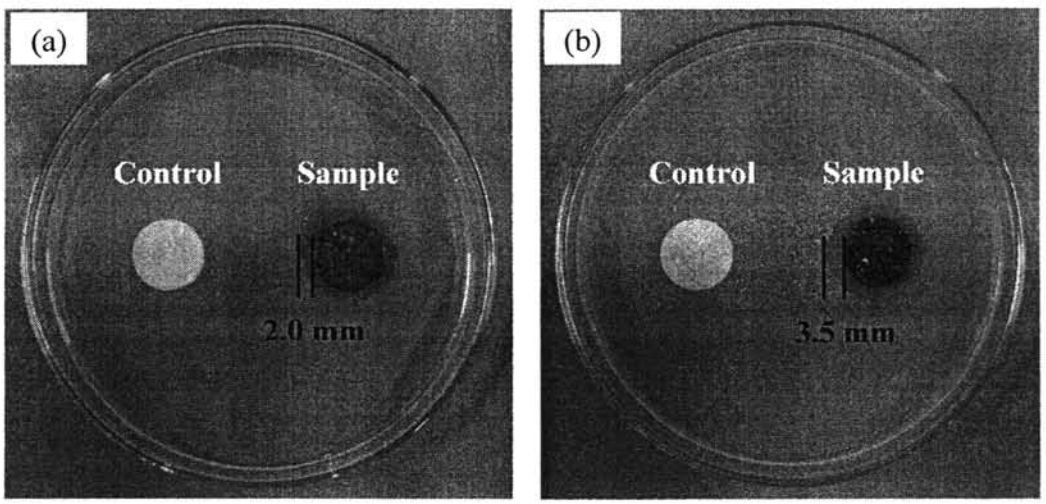

Figure 4.23 Antimicrobial activity of silver nanoparticle-impregnated bacterial cellulose was prepared from the $NaBH_4$:$AgNO_3$ molar ratio of 100:1 against (a) *Escherichia coli* and (b) *Staphylococcus aureus*.

4.7.2 The Colony Forming Count Method

The silver nanoparticle-impregnated bacterial cellulose was tested with *Escherichia coli* and *Staphylococcus aureus*, no bacterial growth was obtained from the sterility control. The viable counts recovered from the silver nanoparticle-impregnated bacterial cellulose before and after incubation were shown in Table 4.3. After 48 hours of incubation, there was a 99.7 % and 99.9 % reduction in viable *Escherichia coli* and *Staphylococcus aureus* on the silver nanoparticle-impregnated bacterial cellulose, respectively. For the pure bacterial cellulose, there was no reduction in viable counts; on the contrary, there was a 34.6 % and 40.7 % increase in the viable counts of *Escherichia coli* and *Staphylococcus aureus*, respectively.

Table 4.3 Colony forming unit counts (cfu/mL) at 0-h and 24-h contact time intervals with the silver nanoparticle-impregnated bacterial cellulose was prepared from the $NaBH_4$: $AgNO_3$ molar ratio of 100: 1 against (a) *Escherichia coli* and (b) *Staphylococcus aureus*

Contact time	*Escherichia coli*		*Staphylococcus aureus*	
	Impregnated BC	Pure BC	Impregnated BC	Pure BC
0 h	1.10×10^5	1.10×10^5	1.50×10^5	1.50×10^5
24h	3.42×10^2	1.48×10^5	1.40×10^2	2.20×10^5
%of reduction/ increase	99.7% reduction	34.6 % increase	99.9% reduction	40.7 % increase

This clearly shows that the silver nanoparticle-impregnated bacterial cellulose has a good antimicrobial activity for both *Escherichia coli* (Gram-negative bacteria) and *Staphylococcus aureus* (Gram-positive bacteria) but antibacterial activity against *Escherichia coli* is lower than that against *Staphylococcus aureus*, probably due to the difference in cell walls between gram-positive and gram-negative bacteria. The cell wall of gram-negative consists of lipids, proteins and lipopolysaccharides (LPS) that provide effective protection against biocides whereas that of gram-positive does not consists of LPS (Feng *et al.*, 2000).